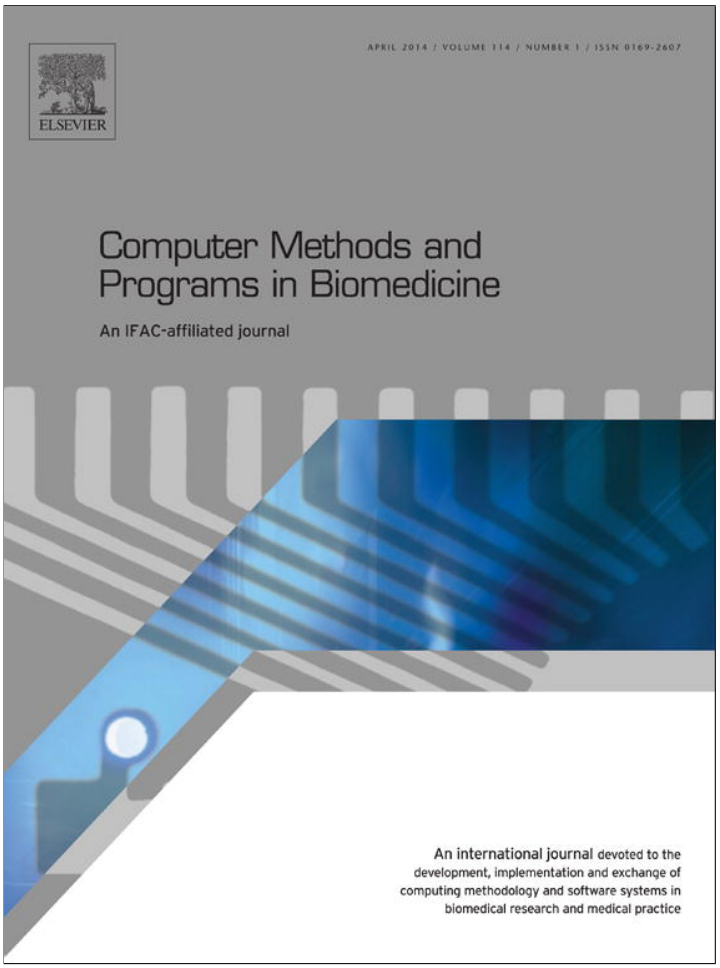

COMPUTER METHODS AND PROGRAMS IN BIOMEDICINE 114 (2014) 109–124

journal homepage: www.intl.elsevierhealth.com/journals/cmpb

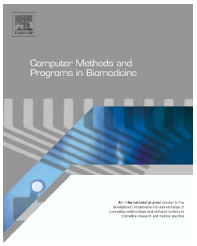

Despeckle filtering software toolbox for ultrasound imaging of the common carotid artery

Christos P. Loizou[a,b,*], *Charoula Theofanous*[b], *Marios Pantziaris*[c], *Takis Kasparis*[b]

[a] *Department of Computer Science, Intercollege, Limassol, Cyprus*
[b] *Department of Electrical Engineering, Computer Engineering & Informatics, Cyprus University of Technology, Limassol, Cyprus*
[c] *Cyprus Institute of Neurology and Genetics, Nicosia, Cyprus*

ARTICLE INFO

Article history:
Received 3 August 2013
Received in revised form
24 November 2013
Accepted 27 January 2014

Keywords:
Despeckling
Speckle
Ultrasound
Image
Carotid artery
Texture analysis

ABSTRACT

Ultrasound imaging of the common carotid artery (CCA) is a non-invasive tool used in medicine to assess the severity of atherosclerosis and monitor its progression through time. It is also used in border detection and texture characterization of the atherosclerotic carotid plaque in the CCA, the identification and measurement of the intima-media thickness (IMT) and the lumen diameter that all are very important in the assessment of cardiovascular disease (CVD). Visual perception, however, is hindered by speckle, a multiplicative noise, that degrades the quality of ultrasound B-mode imaging. Noise reduction is therefore essential for improving the visual observation quality or as a pre-processing step for further automated analysis, such as image segmentation of the IMT and the atherosclerotic carotid plaque in ultrasound images. In order to facilitate this preprocessing step, we have developed in MATLAB® a unified toolbox that integrates image despeckle filtering (IDF), texture analysis and image quality evaluation techniques to automate the pre-processing and complement the disease evaluation in ultrasound CCA images. The proposed software, is based on a graphical user interface (GUI) and incorporates image normalization, 10 different despeckle filtering techniques (DsFlsmv, DsFwiener, DsFlsminsc, DsFkuwahara, DsFgf, DsFmedian, DsFhmedian, DsFad, DsFnldif, DsFsrad), image intensity normalization, 65 texture features, 15 quantitative image quality metrics and objective image quality evaluation. The software is publicly available in an executable form, which can be downloaded from http://www.cs.ucy.ac.cy/medinfo/. It was validated on 100 ultrasound images of the CCA, by comparing its results with quantitative visual analysis performed by a medical expert. It was observed that the despeckle filters DsFlsmv, and DsFhmedian improved image quality perception (based on the expert's assessment and the image texture and quality metrics). It is anticipated that the system could help the physician in the assessment of cardiovascular image analysis.

* *Corresponding author at*: Intercollege, 92 Ayias Phylaxeos Str., P.O. Box 51604, CY-3507 Limassol, Cyprus. Tel.: +357 25 381180; fax: +357 25 386982.
E-mail addresses: loizou.c@lim.intercollege.a.c.cy (C.P. Loizou), ct.theofanous@edu.cut.ac.cy (C. Theofanous), panloicy@logosnet.cy.net (M. Pantziaris), takis.kasparis@cut.ac.cy (T. Kasparis).
0169-2607/$ – see front matter © 2014 Elsevier Ireland Ltd. All rights reserved.
http://dx.doi.org/10.1016/j.cmpb.2014.01.018

1. Introduction

In recent years significant technological advancements and progress in image processing have been achieved, however, still a number of factors in the visual quality of images, hinder the automated analysis [1], and disease evaluation [2]. These include imperfections of image acquisition instrumentations, natural phenomena, transmission errors, and coding artifacts, which all degrade the quality of image in the form of induced noise [3–5]. Ultrasound imaging is a powerful non-invasive diagnostic tool in medicine, but it is degraded by a form of multiplicative noise (speckle), which makes visual observation difficult [4,5]. Speckle is mainly found in echogenic areas of the image in the form of a granular appearance that affects texture of the image [1,6], which may carry important information about the shape of tissues and organs. Texture [2,7,8] and morphology [9] may provide additional quantitative information of the area under investigation, which may complement the human evaluation and provide additional diagnostic details. It is therefore of interest for the research community to investigate and apply new image despeckle filtering techniques that can increase the visual perception evaluation and further automate image analysis, thus improving the final diagnosis. These techniques are usually incorporated into integrated software for medical image processing applications. It should be however noted, that it is not always desirable to remove speckle noise from the images as it can be considered as a natural tissue effect which may provide additional information, especially in the areas of strain imaging and speckle tracking [10], and methods of ultrasound tissue characterization [11]. We propose in this study an integrated despeckle filtering (IDF) software toolbox (see also Fig. 1 and Fig. 2) for ultrasound image of the common carotid artery (CCA) for preprocessing ultrasound images for further analysis and assessment by the medical experts in cardiovascular imaging based diagnosis. The present work incorporates knowledge and results also presented in previous publications made by our group, where despeckle filtering [3–5], quality evaluation [12], segmentation of the intima-media complex (IMC) [13,14] and the atherosclerotic carotid plaque [15] from ultrasound images of the CCA were investigated. Recently, a video despeckle filtering (VDF) toolbox for medical ultrasound video has been proposed [16] and evaluated on 10 ultrasound videos of the CCA. The VDF toolbox builds up on previous work presented from our group [15,17–19].

In order to quantitatively evaluate the proposed IDF software system, we applied 10 different despeckle filtering techniques and evaluated their performance on 100 ultrasound images of the CCA. The IDF software toolbox was furthermore evaluated through 65 different texture features and 15 image quality metrics, which were extracted from the original and the despeckled images as well as through visual perception, performed by a neurovascular specialist, before and after despeckle filtering.

There are a number of studies reported in the literature, where ultrasound image medical software systems have been introduced. An overview of these systems is given in Table 1. The systems tabulated have been grouped under freeware, and other imaging systems. Loizou and Pattichis [4], presented a despeckle filtering study that was accompanied with a despeckle filtering toolbox software for ultrasound imaging of the CCA, based on MATLAB®, whereas, in this paper we extend and make the IDF software publicly available in an executable form, which can be downloaded from http://www.cs.ucy.ac.cy/medinfo/. The other imaging systems in Table 1 cover the despeckling of 2D or 3D ultrasound images, as well as the plaque texture characterization. For ultrasound image denoising, a number of systems are available in the market, such as those that are included in the widely known commercial ultrasound machines (Esaote S.p.A, Philips Electronic Ltd) as well as the ones that can be purchased as stand-alone software systems [20–25].

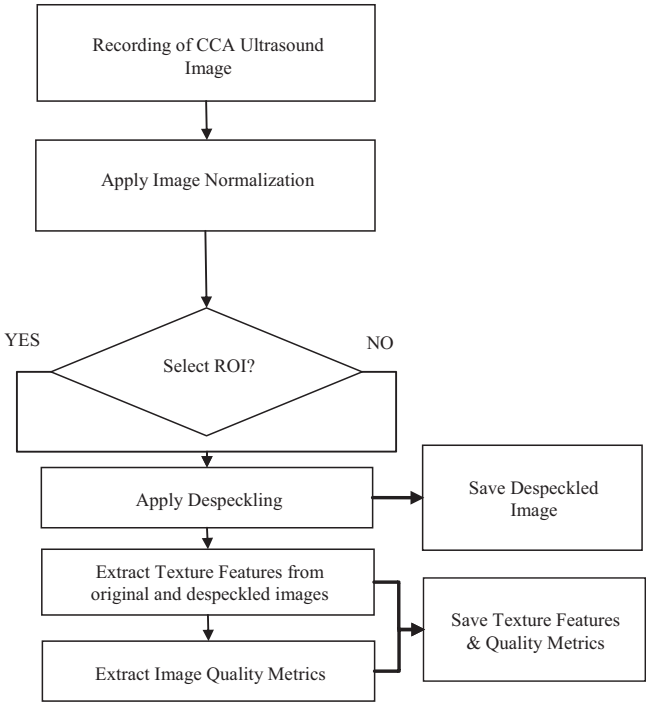

Fig. 1 – Flowchart analysis of the IDF toolbox for ultrasound image analysis.

The structure of the paper is as follows: In Section 2, the theoretical concepts of the proposed image despeckle filters are presented. In Section 3 we provide information on the materials and methods used in this study. The various results are presented in Section 4, followed by discussion (Section 5). Finally, Section 6 concludes the paper.

2. Image despeckle filters

In this section, theoretical background on 10 image despeckle filtering methods used in the proposed IDF software is presented as follows: (a) linear filter (DsFlsmv), (b) Wiener linear filter (DsFwiener), (c) linear filter (DsFlsminsc), (d) nonlinear filter (DsFkuwahara), (e) geometric filter (DsFgf), (f) median filter (DsFmedian), (g) hybrid median filter (DsFhmedian), (h) anisotropic diffusion filter (DsFad), (i) coherent nonlinear anisotropic diffusion filter (DsFnldif), and (j) speckle reducing anisotropic diffusion filter (DsFsrad).

Table 1 – An overview of selected ultrasound common carotid artery imaging despeckling software systems.

Principal investigator	Year	Method	2D/3D	Software platform	N	System features
Freeware imaging systems-despeckling						
Loizou [4,5,12]	2005, 2006, 2008	Despeckle image filtering	2D	Matlab®	440	TIF, JPG, PNG, Matlab® files. Manual, automated segmentation, image normalization, selection of despeckle filtering, texture and image quality analysis. ROI processing.
Imaging systems-despeckling						
Usimagtool® [25]	2007	Image analysis	2D/3D	C++	–	DICOM, Voluson, raw, TIF, JPG, VTK. Additive filtering, edge detection, automated segmentation, volume visualization.
Xu [24]	2008	Ultra3D®, 3D analysis	3D	Windows	–	TIF, JPG, PNG, image acquisition, 3D image reconstruction, image pre-processing, 3D visualization.
Segment™, Phillips Electronics Ltd [21]	2010	Cardiovascular analysis	2D/3D	Windows/Matlab®	–	DICOM, raw, TIF, JPG, ROI manual and automated segmentation.
Imaging systems-plaque segmentation and texture characterization						
Kyriakou [22]	2007	Normalization and plaque texture analysis	2D	Matlab®	440	Supports all image types. Manual segmentation, image normalization, texture analysis.

N: Number of cases investigated.

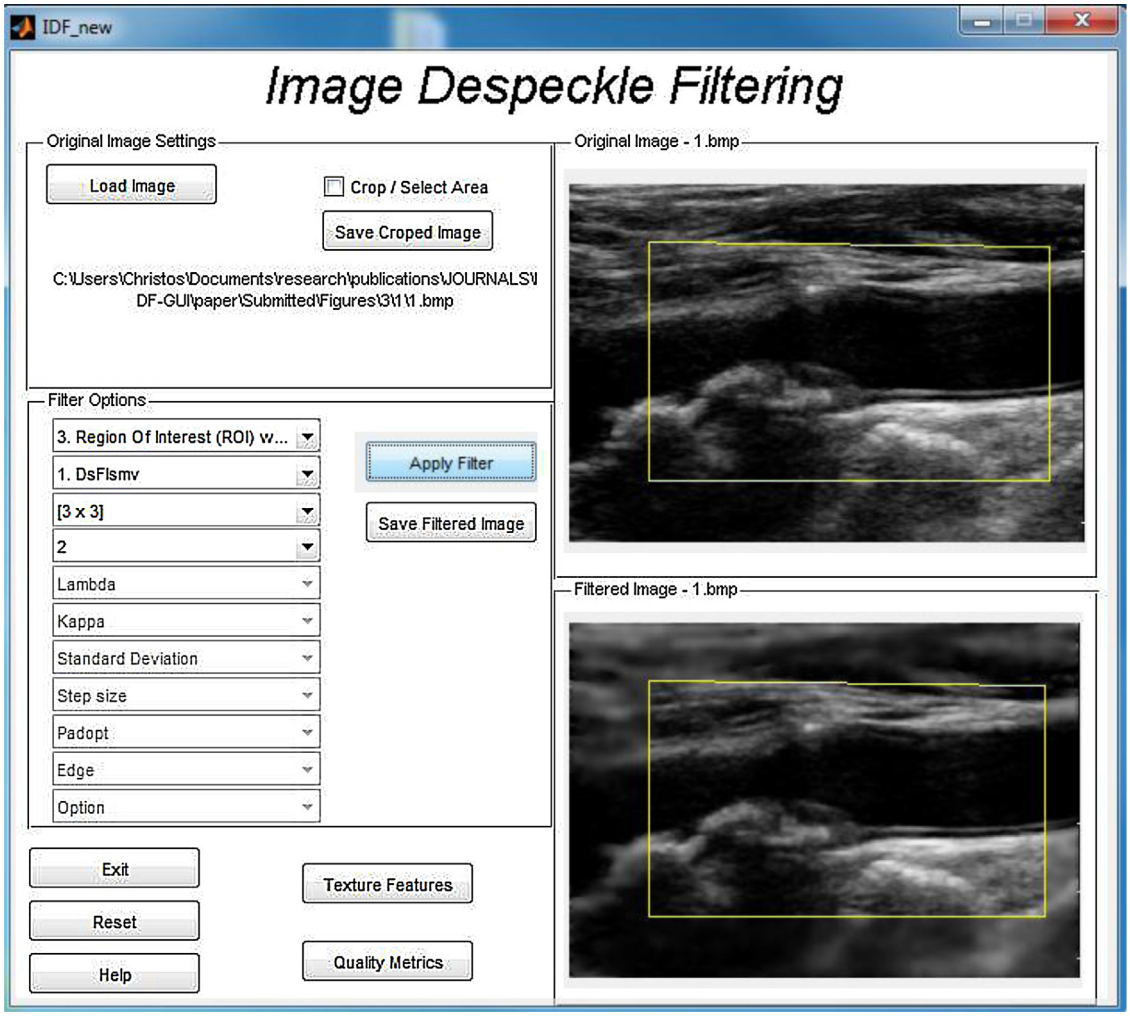

Fig. 2 – The GUI of the proposed IDF toolbox for ultrasound image analysis when filtering is applied in an ROI selected by the user of the system. The following components are shown: original image display, filter options, despeckled image display, texture analysis and quality analysis.

Further algorithmic implementation details and coding can be found in [4,5]. These filters can either be applied to the entire image or to a region of interest (ROI) that can be user specified. The number of iterations, the filtering window size and other filtering parameters that are used for each despeckle filtering method were tuned based, on the subjective despeckled video evaluation by a medical expert (see also Section 3).

2.1. *Linear despeckle filter (DsFlsmv)*

These filters utilize first order statistics such as the variance and the mean of a pixel neighborhood and may be described by a multiplicative noise model [4,5,26] as in (1). Hence the algorithms in this class are mostly based on the following equation:

$$f_{i,j} = \bar{g} + k_{i,j}(g_{i,j} - \bar{g}) \quad (1)$$

where $f_{i,j}$, is the estimated noise-free pixel value, $g_{i,j}$, is the noisy pixel value in the moving window, $\bar{g}$, is the local mean value of an $N_1 \times N_2$ region surrounding and including pixel $g_{i,j}$, $k_{i,j}$ is a weighting factor, with $k \in [0, 1]$, and i, j are the pixel coordinates. The factor $k_{i,j}$, is a function of the local statistics in a moving window and is defined [5,12,26] as:

$$k_{i,j} = \frac{1 - \bar{g}^2\sigma^2}{\sigma^2 + \sigma_n^2}. \quad (2)$$

The values σ^2, and σ_n^2, represent the variance in the moving window and the variance of noise in the whole image respectively. The noise variance may be calculated from the logarithmically compressed image by computing the average noise variance over a number of windows with dimensions considerably larger than the filtering window [5,26]. The moving window size for the despeckle filter DsFlsmv in this study was 5×5 and the number of iterations applied to each image was two. The DsFlsmv filter is the most appropriate in increasing the optical perception evaluation in ultrasound images and videos, while the mean and the median values are preserved in ultrasound images [5] and videos [19] by increasing the optical perception evaluation. The filter decreases the variance of speckle noise in the image, improves statistical and texture

features extraction, increases the classification accuracy and the overall image quality of the image by enhancing edges [4].

2.2. Wiener despeckle filter (DsFwiener)

The filter DsFwiener uses a pixel-wise adaptive Wiener method [4,5,27] implemented as given in (1), with the weighting factor $k_{i,j}$, as follows:

$$k_{i,j} = \frac{\sigma^2 - \sigma_n^2}{\sigma^2}. \quad (3)$$

The moving window size for the despeckle filter DsFwiener in this study was 5×5 and the number of iterations applied to each image was set to one. The DsFwiener filter may be used to increase the optical perception evaluation in ultrasound imaging, but it doesn't preserve edges when compared with the DsFlsmv filter. It is also not well suited for statistical analysis as well as for improving the classification accuracy [4].

2.3. Linear despeckle filter (DsFlsminsc)

The DsFlsminsc is a 2D filter operating in a 5×5 pixel neighborhood by searching for the most homogenous neighborhood area around each pixel using a 3×3 subset window [4,5]. The middle pixel of the 5×5 neighborhood is substituted with the average gray level of the 3×3 mask with the smallest speckle index, C, where C for log-compressed images is given by:

$$C = \frac{\sigma_s^2}{\bar{g}_s} \quad (4)$$

where σ_s^2, and $\bar{g}_s$, represents the variance and the mean of the 3×3 window. The window with the smallest C is the most homogenous semi-window, which presumably, does not contain any edge. The moving window size for the despeckle filter DsFlsminsc in this study was 5×5 and the number of iterations applied to each image was two. The DsFlsminsc filter is very well suited for improving the outcome of the statistical analysis and the classification accuracy, but it does not well preserve edges and the overall image quality. Repeated application of the filter may extensively smooth the image and the edges of an organ and thus destroying subtle details [4].

2.4. Nonlinear despeckle filter (DsFkuwahara)

The DsFkuwahara is an 1D filter operating in a 5×5 pixel neighborhood searching for the most homogenous neighborhood area around each pixel [4,28]. The middle pixel of the 1×5 neighborhood is then substituted by the median gray level of the 1×5 mask. The filter is iteratively applied to the image where the number of iterations is selected by the user. In this study the number of iterations selected for the despeckle filter DsFkuwahara was set to two. The DsFkuwahara filter can be used to improve the classification accuracy of different organs and tissues and to enhance edges, thus also improving the optical perception evaluation [3].

2.5. Geometric despeckle filter (DsFgf)

The concept in the geometric filtering is that speckle appears in the image as narrow walls and valleys. The geometric filter, through iterative repetition, gradually tears down the narrow walls (bright edges) and fills up the narrow valleys (dark edges), thus smearing the weak edges that need to be preserved. The DsFgf filter [29], uses a non-linear noise reduction technique. It compares the intensity of the central pixel in a 3×3 neighborhood with those of its 8 neighbors, and based upon the neighborhood pixel intensities it increments or decrements the intensity of the central pixel such that it becomes more representative of its surroundings. Further algorithmic details and additional explanation of the operation of the geometric filter DsFgf may be found in [4,5]. The moving window size for the despeckle filter DsFgf in this study was 5×5 and the number of iterations applied to each image was set to one. The DsFgf filter shows very good performance with respect to decreasing the speckle index in the image and for improving the classification success rate of the kNN classifier for the classification of asymptomatic and symptomatic images [4,5].

2.6. Median (DsFmedian), hybrid median (DsFhmedian) despeckle filters

The filter DsFmedian [4,5] is a median filter applied over windows of size 5×5. This is an extension of the filter DsFhmedian, which was introduced in [30] and later used in [4,5] and it computes the median of the outputs generated by median filtering with three different windows (cross shape window, x-shape window and normal window). The moving size window for the despeckle filter DsFmedian and DsFhmedian was for both filters 5×5 pixels, while the number of iterations applied to each image was three and two respectively. The DsFmedian filter is well suited for improving the optical perception evaluation but repeated application destroys the image edges. The filter DsFhmedian preserves the edges and increases the optical perception evaluation. It can thus be used to preserve and enhance edges of various organs in ultrasound images [3,4].

2.7. Anisotropic diffusion filter (DsFad)

Perona and Malik [31] introduced the following function, $d_{i,j,t} = f(|\nabla g|)$, that smoothes the original image while trying to preserve brightness discontinuities:

$$\frac{dg_{i,j,t}}{dt} = div[d_{i,j,t}\nabla g_{i,j,t}] = \left[\frac{d}{di}d_{i,j,t}\frac{d}{di}g_{i,j,t}\right] + \left[\frac{d}{dj}d_{i,j,t}\frac{d}{dj}g_{i,j,t}\right] \quad (5)$$

where $|\nabla g|$, is the gradient magnitude, and $d(|\nabla g|)$, is an edge stopping function, which is chosen to satisfy $d \to 0$ when $|\nabla g| \to \infty$ so that the diffusion is stopped across edges. This function, called the diffusion coefficient, $cd(|\nabla g|)$, is a monotonically decreasing function of the gradient magnitude, $|\nabla g|$, yielding intra-region smoothing, and not inter-region smoothing [4,5,17,27,31] by impeding diffusion at image edges. A basic anisotropic partial-differential equation is given in (5). Two

different diffusion coefficients were proposed in [31], as follows:

$$cd(|\nabla g|) = \frac{1}{1+(|\nabla g_{i,j}|/K)^2}, \text{ and } \quad cd(|\nabla g|) = \frac{2|\nabla g_{i,j}|}{2+(|\nabla g_{i,j}|/K_1)^2} \tag{6}$$

where K and K_1, are positive gradient threshold parameters, known as diffusion or flow constants [31]. In this work we used the first diffusion coefficient in (6) as it was found to perform better in our images [4,5].

A discrete formulation of the anisotropic diffusion in (5) is [4,31]:

$$\frac{dg_{i,j}}{dt} = \frac{\lambda}{|\eta_s|}\{d_{i+1,j,t}[g_{i+1,j}-g_{i,j}] + d_{i-1,j,t}[g_{i-1,j}-g_{i,j}] + d_{i,j+1,t}[g_{i,j+1}-g_{i,j}] + d_{i,j-1,t}[g_{i,j-1}-g_{i,j}]\}, \tag{7}$$

where the new pixel gray value, $f_{i,j}$, at location i, j, is:

$$f_{i,j} = g_{i,j} + \frac{1}{4}\frac{dg_{i,j}}{dt}, \tag{8}$$

where $d_{i+1,j,t}$, $d_{i-1,j,t}$, $d_{i,j+1,t}$, and $d_{i,j-1,t}$, are the diffusion coefficients for the west, east, north and south pixel directions respectively, in a four pixel neighborhood, around the pixel i, j, where diffusion is computed. In regions where the nearest-neighbor difference is larger (large edge), the diffusion coefficient is also large yielding more pronounced diffusion (smoothing), while the opposite is true in regions where the nearest-neighbor difference is smaller (the weakest edge). The constant, $\lambda \in \Re^+$, is a scalar that determines the rate of diffusion while, η_s, represents the spatial neighborhood of pixel, i, j, and $|\eta_s|$, is the number of neighbors (usually 4 neighbors except at the image boundaries). Perona and Malik [31] linearly approximated the directional derivative in a particular direction as, $\nabla g_{i,j} = g_{i+1,j} - g_{i,j}$ (for the east direction of the central pixel i, j). Modifying the image according to equation in (7) (which is essentially a linear isotropic diffusion equation), is equivalent to filtering the image with a Gaussian filter. The parameters for the anisotropic diffusion filter used in this work were, number of iterations 20, $\lambda = 0.25$, $\eta_s = 8$, and the parameter K, which is used for the calculation of the edge stopping function $cd(|\nabla g|)$, in (6) was set equal to $K = 30$. The DsFad filter usually smooths the image extensively but it was observed that it can also be used to improve the quality of video encoding as well reducing the bandwidth required for transmitting the filtered image over a 3G wireless network [32].

2.8. Coherent nonlinear anisotropic diffusion filter (DsFnldif)

The DsFnldif filter use a symmetric positive semi-definite diffusion tensor [33] with the parameters as given in [4]. Therefore, the DsFnldif filter takes the form:

$$\frac{dg_{i,j,t}}{dt} = div[D\nabla g] \tag{9}$$

where $D \in \Re^{2x2}$, is a symmetric positive semi-definite diffusion tensor representing the required diffusion in both gradient and contour directions and, hence, enhancing coherent structures as well as edges. The design of D, as well as the derivation of the coherent nonlinear anisotropic diffusion model may be found in [33] and is given as:(10)$D = (\omega_1\ \omega_2)\begin{pmatrix}\lambda_1 & 0\\ 0 & \lambda_2\end{pmatrix}\begin{pmatrix}\omega_1^T\\ \omega_2^T\end{pmatrix}$ with

$$\lambda_1 = \begin{cases}\alpha\left(1-\frac{(\mu_1-\mu_2)^2}{s^2}\right) & \text{if } (\lambda_1-\lambda_2)^2 \le s^2\\ 0, & \text{else}\end{cases} \tag{11}$$

$$\lambda_2 = \alpha.$$

where the eigenvectors ω_1, ω_2 and the eigenvalues λ_1, λ_2 of η_s correspond to the directions of maximum and minimum variations and the strength of these variations, respectively. The flow at each point is affected by the local coherence, which is measured by $(\mu_1 - \mu_2)$ in (11). The parameters used in this work for the DsFnldif filter were, $s^2 = 2$, and $\alpha = 0.9$, which were used for the calculation of the diffusion tensor D, and the parameter step size $m = 0.2$, which defined the number of diffusion steps performed. The local coherence is close to zero in very noisy regions and diffusion becomes isotropic ($\mu_1 = \mu_2 = \alpha = 0.9$), whereas in regions with lower speckle noise the local coherence corresponds to $(\mu_1 - \mu_2)^2 > s^2$ [33]. The number of iterations applied to each image, selected in this study, for the DsFnldif filter was 5. As it was shown in [3], the DsFnldif filter may be used to improve the visual appearance of clinical structures and to improve the atherosclerotic carotid plaque borders in ultrasound images.

2.9. Speckle reducing anisotropic diffusion filter (DsFsrad)

Speckle reducing anisotropic diffusion is described in [33]. It is based on setting the diffusion coefficient in the diffusion equation (5) using the local frame gradient and the frame Laplacian. The DsFsrad filter in [33] uses two seemingly different methods, namely the Lee [26] and the Frost diffusion filters [27]. In [33], a more general updated function for the output image is presented, by extending the PDE versions of the despeckle filter as:

$$f_{i,j} = g_{i,j} + \frac{1}{\eta_s} div(c_{srad}(|\nabla g|)\nabla g_{i,j}). \tag{12}$$

where η_s is the size of the filtering window. The diffusion coefficient for the speckle anisotropic diffusion, $c_{srad}(|\nabla g|)$, is given in [33] as:

$$c^2_{srad}(|\nabla g|) = \frac{(1/2)|\nabla g_{i,j}|^2 - (1/16)(\nabla^2 g_{i,j})^2}{(g_{i,j} + (1/4)\nabla^2 g_{i,j})^2}. \tag{13}$$

It is required that $c_{srad}(|\nabla g|) \ge 0$. The above instantaneous coefficient of variation combines a normalized gradient magnitude operator and a normalized Laplacian operator to act like an edge detector. High relative gradient magnitude and

low relative Laplacian indicates an edge. The DsFsrad filter utilizes speckle reducing anisotropic diffusion according to (12) with the diffusion coefficient, $c_{srad}(|\nabla g|)$ in (13) [33]. The coefficient of variation for the DsFsrad filter can be selected from 0.01 up to 0.1 and the number of iterations from 1 to 200. In this study the number of iterations applied to each image, was set to 30, while the coefficient of variation was 0.02. As it was observed during the processing of the carotid plaque borders and the IMC in ultrasound images and videos, [3–5,12–19], the DsFsrad filter may be used to improve the overall image quality. It was furthermore observed to improve the quality of video encoding as well reducing the bandwidth required for transmitting the filtered ultrasound image over a 3G wireless network [32].

3. Despeckle filtering toolbox for ultrasound image

The proposed IDF software toolbox, implementation is capable of loading image files of most popular standards (see also Fig. 1). The image analysis usually starts by importing the original ultrasound image of the CCA (and subsequently defining an ROI in the image) where despeckle filtering will be applied. There are 65 different texture features and 15 image quality metrics that can be extracted and evaluated by comparing the original and despeckled images.

Fig. 1 presents a flowchart analysis of the proposed integrated ultrasound IDF software system, where the different modules of the software are outlined, while Fig. 2 presents the graphical user interface (GUI) of the system.

3.1. *Recording of ultrasound images*

A total of 100 B-mode longitudinal ultrasound images of the CCA (see Figs. 3 and 4), from women and men used for despeckling, were recorded using the ATL HDI-5000 ultrasound scanner (Advanced Technology Laboratories, Seattle, WA), [34]. The ATL HDI-5000 scanner is equipped with a 256 elements fine pitch high-resolution 50 mm linear array, a multi element ultrasound scan head with an extended operating frequency range of 5–12 MHz and it offers real spatial compound imaging. The scanner increases the image clarity using SonoCT imaging by enhancing the resolution and borders, and interface margins are better displayed. Several tests made by the manufacturer showed that the ATL HDI-5000 scanner performance was overall superior compared to conventional 2D imaging systems, primarily because of the reduction of speckle, contrast resolution, tissue differentiation, and image visual quality [3–5,12–19].

Digital images were resized using the bicubic method to a standard pixel density of 16.66 pixels/mm with a resolution of 0.06 mm. This was carried out due to the small variations in the number of pixels per mm of image depth (i.e., for deeply situated carotid arteries, image depth was increased, and therefore, digital image spatial resolution would have decreased) and to maintain uniformity in the digital image spatial resolution [9]. The images were logarithmically compressed and were recorded digitally on a magneto optical drive at 768 × 576 pixels with 256 gray levels at the Cyprus Institute of Neurology and Genetics, in Nicosia, Cyprus. The subjects were, 42 female and 58 male asymptomatic aged between 26 and 95 years old, with a mean age of 54 years that had not developed clinical symptoms, such as a stroke or a transient ischemic attack (TIA).

3.2. *Ultrasound image normalization*

Brightness adjustments of ultrasound images (see Figs. 3 and 4) can be carried out based on the method introduced in [2], which improves image compatibility by reducing the variability introduced by different gain settings, different operators, different equipment, and facilitates ultrasound tissue comparability [9]. Algebraic (linear) scaling of the entire image is manually performed by linearly adjusting the image so that the median gray level value of the blood was 0–5, and the median gray level of the adventitia (artery wall) was 180–190 [2,35]. The scale of the gray level of the images ranged from 0–255. Thus the brightness of all pixels in the image is readjusted according to the linear scale defined by selecting the two reference regions. It is noted that a key point to maintaining a high reproducibility was to ensure that the ultrasound beam was at right angles to the adventitia, adventitia which was visible adjacent to the plaque and that for image normalization a standard sample consisting of the half of the width of the brightest area of adventitia was obtained.

3.3. *Application of despeckle filtering*

Despeckle filtering can be applied either to the entire image (see also Fig. 3) or to an ROI, (see also Fig. 4) selected by the user after image normalization (see Section 3.2). The selected ROI can be of any shape but the software doesn't support multiple ROIs selection. In the latter case, where the user of the system is interested only in the selected ROI, the area outside the ROI can be blurred using the DsFlsmv filter operating with a sliding moving window of 15 × 15 pixels and a number iterations 5 (see also Fig. 4). It should be noted that the blurring is applied outside of the ROI if the user of the system is not interested to subjectively evaluate this area. The input parameters of the 10 different despeckle filters for the IDF software tool can be selected by the user as it was documented in Section 2 earlier.

3.4. *Texture feature analysis*

Texture provides useful information for the characterization of CCA [7]. The proposed IDF system (see Figs. 1 and 2) is able to extract, and save in a separate file, a total of 65 different texture features both from the original and the despeckled images which are the following [7]:

(i) Statistical Features (SF): (1) Mean, (2) Median, (3) Variance (σ^2), (4) Skewness (σ^3), and (5) Kurtosis (σ^4).
(ii) Spatial Gray Level Dependence Matrices (SGLDM) as proposed by [8]: (1) Angular second moment (ASM), (2) Contrast, (3) Correlation, (4) Sum of squares variance (SOSV), (5) Inverse difference moment (IDM), (6) Sum average (SA), (7) Sum variance (SV), (8) Sum entropy (SE), (9) Entropy, (10) Difference variance (DV), (11) Difference entropy (DE), (12), and (13) Information measures of

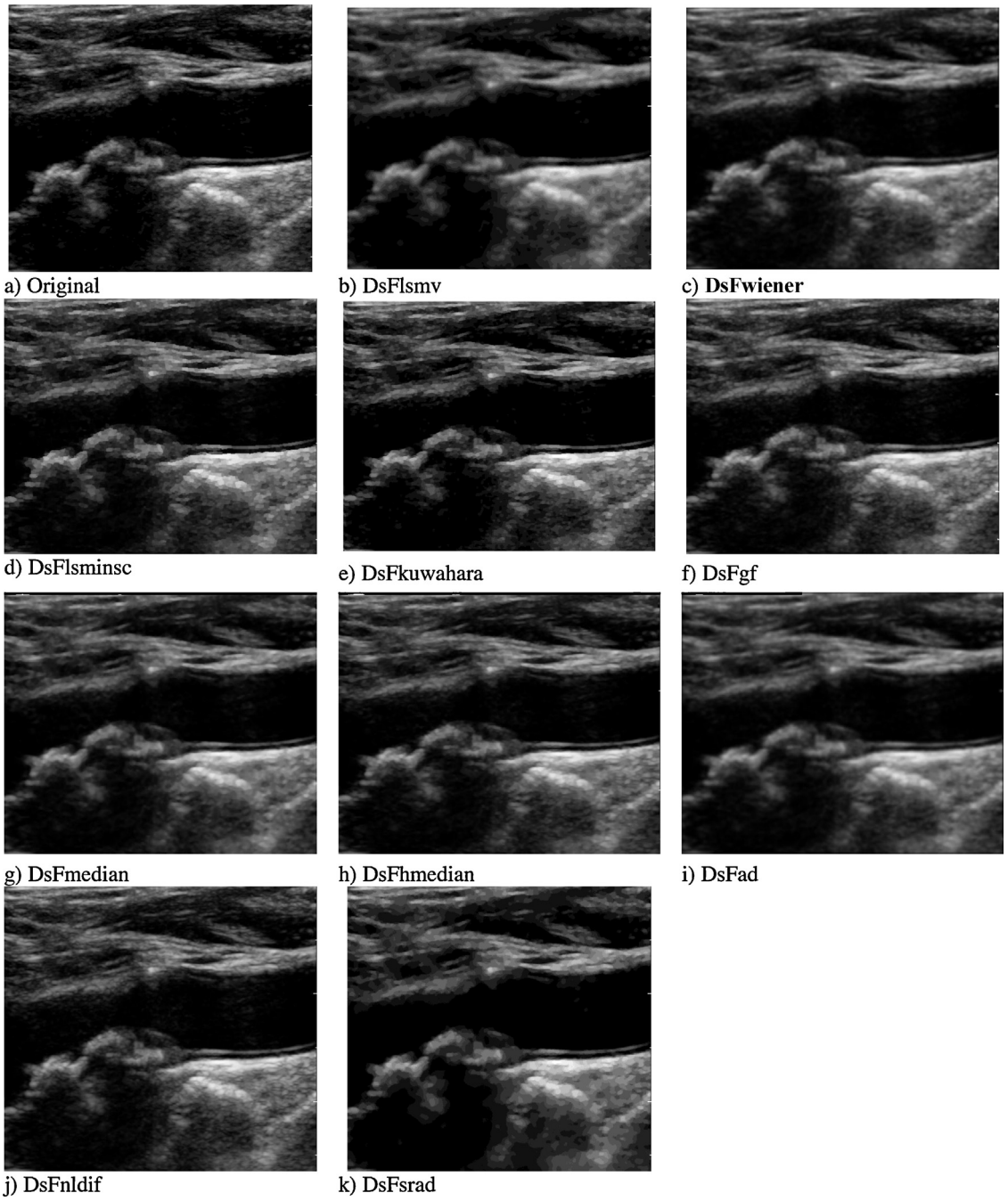

Fig. 3 – Examples of despeckle filtering on the whole ultrasound image of the CCA acquired from a female asymptomatic subject at the age of 63 with 53% stenosis and a plaque at the far wall of the CCA for the: (a) original, (b) DsFlsmv, (c) DsFwiener, (d) DsFlsminsc, (e) DsFkuwahara, (f) DsFgf, (g) DsFmedian, (h) DsFhmedian, (i) DsFad, (j) DsFnldif and (k) DsFsrad.

correlation. For a chosen distance d (in this work $d = 1$ was used) and for angles $\theta = 0^\circ$, 45°, 90°, and 135°, we computed four values for each of the above texture measures. Each feature was computed using a distance of one pixel. Then for each feature the mean values and the range of values were computed, and were used as two different feature sets.

(iii) Gray level difference statistics (GLDS) [36]: (1) homogeneity, (2) contrast, (3) energy, (4) entropy, and (5) mean. The above features were calculated for displacements $\delta = (0, 1)$, (1, 1), (1, 0), (1, −1), where $\delta \equiv (\Delta x, \Delta y)$, and their mean values were taken.

(iv) Neighborhood gray tone difference matrix (NGTDM) [37]: (1) coarseness, (2) contrast, (3) busyness, (4) complexity, and (5) strength.

(v) Statistical feature matrix (SFM) [6]: (1) coarseness, (2) contrast, (3) periodicity, and (4) roughness.

(vi) Laws texture energy measures (LTEM) [6]: (1) LL-texture energy from LL kernel, (2) EE-texture energy from EE-kernel, (3) SS-texture energy from SS-kernel,

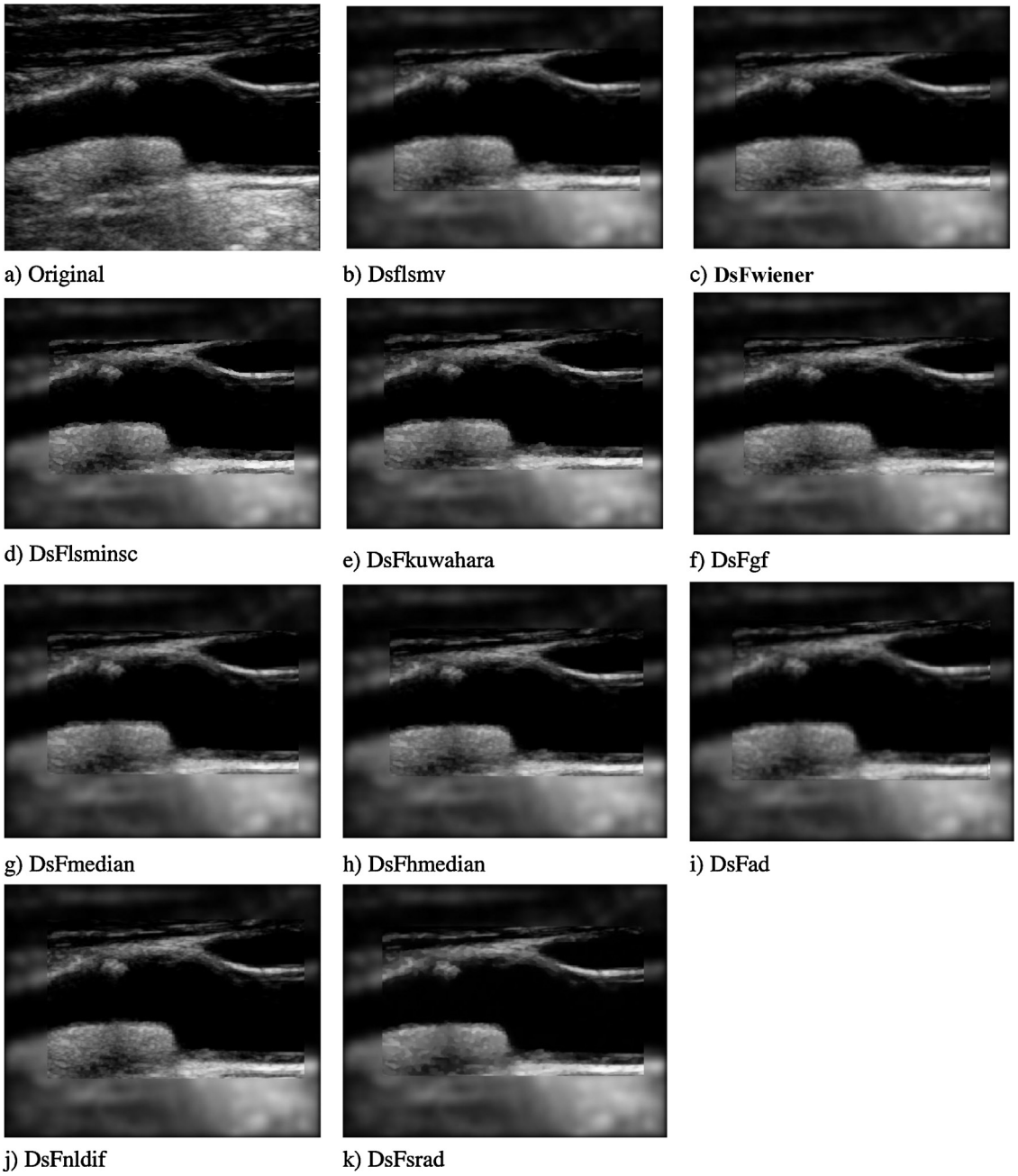

Fig. 4 – Examples of despeckle filtering in an ROI selected by the user of the system, of an ultrasound image of the CCA acquired from a male symptomatic subject at risk of atherosclerosis with a stenosis of 65% and a plaque at the far wall of the CCA for the: (a) original, (b) DsFlsmv, (c) DsFwiener, (d) DsFlsminsc, (e) DsFkuwahara, (f) DsFgf, (g) DsFmedian, (h) DsFhmedian, (i) DsFad, (j) DsFnldif and (k) DsFsrad.

(4) LE-average texture energy from LE and EL kernels, (5) ES-average texture energy from ES and SE kernels, and (6) LS-average texture energy from LS and SL kernels.

(vii) Fractal dimension texture analysis (FDTA) [6]: The Hurst coefficients for dimensions 4, 3 and 2 were computed.

(viii) Fourier Power Spectrum (FPS) [6]: (1) radial sum, and (2) angular sum.

(ix) Shape parameters: (1) X-coordinate maximum length, (2) Y-coordinate maximum length, (3) area, (4) perimeter, (5) perimeter^2/area, (6) eccentricity, (7) equivalence diameter, (8) major axis length, (9) minor axis length, (10) centroid, (11) convex area, and (12) orientation.

3.5. *Image quality metrics*

Objective image quality assessment is an emerging area of active research [1]. In order to quantitatively assess the original and despeckled images, differences between the original and the processed images were evaluated using image quality and evaluation metrics, which were used as statistical

measures. The basic idea is to compute a single number that reflects the quality of the processed image. Processed images with higher metrics have been evaluated as being better [1]. The following 15 different quality evaluation measures, which are easy to compute and have clear physical meaning, were computed [3–5,12]: (a) geometric average error, (b) mean square error (MSE), (c) signal-to-noise ratio (SNR), (d) mean root square error (MRSE), (e) peak signal-to-noise ratio (PSNR), (f, g) error summation in the form of the Minkowski metric (Err1, Err2), (h) universal quality index (Q), (i) Structural similarity index (SSI), (j) average difference (AD), (k) Structural content (SC), (l) normalized cross-correlation (NCC), (m) maximum difference (MD), (n) Laplacian mean square error (LMSE), and (o) normalized absolute error (NAE). A complete description of the above metrics can be found in [5,12] as well as their MATLAB® software implementation in [4].

3.6. *Visual evaluation by the expert*

In order to objectively evaluate the proposed system, the 100 ultrasound images of the CCA, after image normalization and speckle reduction filtering using MATLAB® software developed by our group, were visually inspected (see Sections 3.2 and 3.3) by a neurovascular specialist. For each case, the original and the normalized despeckled images (despeckled with filters DsFlsmv, DsFwiener, DsFlsminsc, DsFkuwahara, DsFgf, DsFmedian, DsFhmedian, DsFad, DsFnldif, DsFsrad) were presented blindly at random to the expert. The expert was asked to assign a score corresponding to low and high subjective visual perception criteria in a scale from one to ten, the latter was given to the best visual perception. Therefore, if the expert assigned the score of 10 for all the 100 images, the maximum score for that filter is 1000. The expert was also allowed to give equal scores to more than one image in each case. For each class and for each filter the average score was computed. The expert evaluated the area around the IMC, 2–3 cm before the bifurcation and the bifurcation around the IMC borders. It should also be noted that the scoring system used in this work pre-assumes an a priori knowledge of the range of the quality of the images, therefore the expert inspected all 100 images in random order before scoring.

4. Results

4.1. *Examples using the despeckle filtering toolbox for ultrasound images*

The applicability of the IDF software toolbox was evaluated based on normalization, despeckle filtering, texture features, image quality evaluation metrics and visual perception evaluation made by a medical expert.

Fig. 3(a) illustrates an original ultrasound image of the CCA with an atherosclerotic plaque at the far wall, acquired from an asymptomatic female subject at the age of 63 and a stenosis of 53%. Fig. 3(b)–(k) presents the despeckled images (filtering applied to the entire image), with the 10 different filters, namely (DsFlsmv, DsFwiener, DsFlsminsc, DsFkuwahara, DsFgf, DsFmedian, DsFhmedian, DsFad, DsFnldif and DsFsrad). It can be observed that the filters DsFlsmv and DsFhmedian smoothed the image without destroying subtle details.

Fig. 4 presents a different ultrasound image of the CCA acquired from a symptomatic subject at risk of atherosclerosis with a stenosis of 65% and a plaque at the far wall of the CCA, where the 10 different despeckle filters are applied in an ROI, selected by the user. The area outside of the ROI is blurred with the DsFlsmv filter. It is again observed that filters DsFlsmv and DsFhmedian smoothed the image without destroying subtle details. The average processing time is about 2–3 s per image (on an Intel Core i5-3470 processor with 3.2 GHz and 1GByte of RAM) for the image despeckling.

4.2. *Texture feature analysis*

Since texture features data are not normally distributed, the Wilcoxon rank sum test [38] which calculates the difference between the sum of the ranks of two independent samples, may be used to identify whether significant difference (S) or not (NS) between sets of texture features extracted from the original and the despeckled images exists, with a confidence level of 95% ($p < 0.05$).

Table 2 presents the results of selected texture features (see Section 3.4), extracted from the entire original and the despeckled images and from an ROI (–/–), that was selected, showing significance difference after despeckle filtering ($p < 0.05$). The features were extracted from all 100 ultrasound images of the CCA investigated in this study. These features were the median, variance (SF feature group), sum average (SGLDM range of values feature group), contrast (GLDM feature group), coarseness, busyness (NGTDM feature group), roughness (SFM feature group), energy LL kernel (LTEM feature group), Hoerst coefficient H1 (FD feature group) and angular sum (FPS feature group). Also, the number of iterations (no. of it.) for each filter, which was selected based on C (see Eq. (4)) and on the visual evaluation of the expert, is given in the second row of Table 2. When C was minimally changing, the filtering process was stopped. It is observed from Table 2 that almost all filters preserve the median and reduce the variance. Furthermore, it is also observed that when the DsFlsmv and DsFKuwahara filters are applied to the whole image, they increase contrast, H1 and angular sum, but lower roughness while at the same time they preserve the rest of the features. The results of this study can also be favorably compared with the results presented in [5,12], where similar texture features values were computed for the DsFlsmv despeckled plaque images.

4.3. *Image quality metrics*

Table 3 tabulates selected image quality metrics between original and despeckled images when filtering is applied on the entire image and when applied in an ROI (–/–). For all filters investigated, when filtering was applied on the entire image or in an ROI the geometric average error (GAE) was 0. This can be attributed to the fact that the information between the original and the processed images remains unchanged. The quality metrics LMSE, and NAE showed a similar performance as the MSE and RMSE whereas for the DsFlsmv filter, smaller values of the same metrics were observed. It is observed from

Table 2 – Texture features (mean ± sd), that showed significant diference (using the wilcoxon rank sum test at $p < 0.05$) after despeckle filtering, for all 100 images of the CCA extracted from the original and the despeckled images from the whole image and the roi (–/–).

	Original	DsFlsmv	DsFwiener	DsFlsminsc	DsFkuwahara	DsFgf	DsFmedian	DsFhmedian	DsFad	DsFnldif	DsFsrad
No. of it.		2	1	2	2	1	3	2	20	5	30
Statistical features (SF)											
Median	43 ± 14/	43 ± 11/	45 ± 12/	40 ± 12/	43 ± 14/	41 ± 11/	40 ± 10/	43 ± 14/	39 ± 9/	41 ± 12/	43 ± 13/
	23 ± 17	23 ± 15	21 ± 15	20 ± 15	26 ± 17	21 ± 14	19 ± 13	25 ± 12	19 ± 13	21 ± 15	26 ± 14
Variance	54 ± 6/	53 ± 5/	47 ± 4/	50 ± 7/	58 ± 8/	50 ± 4/	49 ± 14/	54 ± 6/	48 ± 5/	43 ± 7/	54 ± 5/
	58 ± 8	58 ± 7	55 ± 7	56 ± 9	26 ± 17	55 ± 7	55 ± 9	58 ± 8	51 ± 6	50 ± 7	62 ± 8
SGLDM range of values–spatial gray level dependence matrix											
Sum average	0.3 ± 0.1/	0.4 ± 0.2/	0.3 ± 0.3/	0.5 ± 0.2/	0.4 ± 0.2/	0.4 ± 0.3/	0.3 ± 0.1/	0.4 ± 0.2/	0.2 ± 0.1/	0.3 ± 0.2/	0.4 ± 0.3/
	0.9 ± 0.7	0.2 ± 0.2	55 ± 7	06 ± 0.9	0.4 ± 0.2	0.8 ± 0.4	0.6 ± 0.1	0.5 ± 0.3	0.6 ± 0.4	0.5 ± 0.3	0.5 ± 0.4
GLDS-gray level difference statistics											
Contrast	118 ± 34/	122 ± 31/	112 ± 29/	115 ± 31/	134 ± 30/	148 ± 29/	71 ± 14/	75 ± 13/	110 ± 14/	111 ± 17/	116 ± 31/
	119 ± 34	120 ± 17	110 ± 16	116 ± 17	108 ± 31	155 ± 22	23 ± 17	73 ± 17	55 ± 11	61 ± 16	70 ± 19
NGTDM-neighborhood gray tone difference matrix											
Coarseness	39 ± 7/	92 ± 13/	33 ± 6/	41 ± 5/	37 ± 4/	30 ± 9/	41 ± 10/	**52 ± 11**/	50 ± 17/	49 ± 13/	54 ± 22/
	61 ± 11	110 ± 22	76 ± 12	74 ± 13	55 ± 12	88 ± 14	23 ± 17	**84 ± 21**	29 ± 14	24 ± 12	33 ± 18
Busyness	3 ± 8.5/	1.2 ± 3.7/	3.2 ± 4/	3 ± 6.7/	3.7 ± 3.8/	2.9 ± 7.4/	4.3 ± 14/	2.1 ± 5.7/	4.3 ± 1.4/	2.1 ± 1.4/	2.4 ± 9.4/
	2.7 ± 9.5	1.3 ± 5.85	1.9 ± 9.2	2.2 ± 8.1	2.7 ± 1.1	2.3 ± 9.2	2.7 ± 9.5	1.7 ± 4.1	5.1 ± 2.3	5.5 ± 2.4	5.7 ± 2.9
SFM-statistical feature matrix											
Roughness	2.2 ± 0.02/	2.1 ± 0.01/	2.2 ± 0.04/	1.9 ± 0.03/	2.1 ± 0.01/	2.1 ± 0.04/	2.3 ± 0.01/	2.1 ± 0.07/	2.3 ± 0.04/	2.1 ± 0.02/	2.2 ± 0.03/
	2.2 ± 0.02	2.1 ± 0.01	1.9 ± 0.04	1.9 ± 0.02	2.1 ± 0.01	2.3 ± 0.02	2.2 ± 0.02	2.1 ± 0.03	2.1 ± 0.03	2.1 ± 0.01	2.3 ± 0.09
LTEM-laws texture energy measures											
Energy	367 ± 47/	343 ± 20/	312 ± 49/	215 ± 22/	445 ± 49/	148 ± 29/	271 ± 16/	298 ± 26/	290 ± 34/	297 ± 37/	310 ± 36/
LL-Kernel	233 ± 34	226 ± 28	220 ± 36	216 ± 17	382 ± 41	255 ± 32	223 ± 17	244 ± 35	265 ± 31	261 ± 26	275 ± 38
FD-fractal dimension											
H1	0.5 ± 0.02/	0.6 ± 0.007/	0.3 ± 0.03/	0.5 ± 0.02/	0.6 ± 0.006/	0.4 ± 0.03/	0.6 ± 0.001/	0.5 ± 0.02/	0.2 ± 0.01/	0.3 ± 0.02/	0.4 ± 0.08/
	0.9 ± 0.07	0.2 ± 0.2	0.3 ± 0.03	0.6 ± 0.02	0.4 ± 0.002	0.5 ± 0.04	0.6 ± 0.001	0.5 ± 0.03	0.6 ± 0.04	0.5 ± 0.03	0.5 ± 0.4
FPS-Fourier power spectrum											
Angular	189 ± 35/	190 ± 35/	155 ± 17/	116 ± 39/	191 ± 35/	118 ± 44/	196 ± 31/	119 ± 363/	171 ± 34/	165 ± 33/	188 ± 35/
Sumx100	87 ± 21	101 ± 27	83 ± 19	75 ± 22	63 ± 21	64 ± 23	45 ± 11	101 ± 25	102 ± 21	113 ± 19	108 ± 23

H1: Hoerst coefficient.

Table 3 – Image quality evaluation metrics for the 100 ultrasound images of the cca extracted from the original and the despeckled images from the whole image and the roi (–/–).

Feature set	DsFlsmv	DsFwiener	DsFlsminsc	DsFkuwahara	DsFgf	DsFmedian	DsFhmedian	DsFad	DsFnldif	DsFsrad
MSE	6441 ± 1805/ 6168 ± 2149	6433 ± 1821/ 6523 ± 1756	6345 ± 1978/ 6712 ± 2200	6231 ± 1856/ 6183 ± 2153	6578 ± 2179/ 6678 ± 2198	6232 ± 1857/ 6118 ± 1765	6232 ± 1856/ 6183 ± 2153	6567 ± 2133/ 6578 ± 2122	6356 ± 1978/ 6268 ± 1856	6231 ± 1856/ 6114 ± 1990
SNR	31 ± 1.6/ 33 ± 1.3	26 ± 2.2/ 21 ± 2.6	24 ± 2.3/ 21 ± 1.9	17.4 ± 0.8/ 31 ± 3.9	18 ± 2.1/ 11 ± 4.6	28 ± 2.2/ 26 ± 1.9	33 ± 1.1/ 35 ± 2.9	29 ± 1.9/ 21 ± 1.2	30.4 ± 1.6/ 29 ± 2.1	34 ± 4.1/ 34 ± 3.1
RMSE	3.4 ± 0.81/ 2.4 ± 0.56	4.5 ± 4.4/ 4.1 ± 0.32	4.9 ± 4.7/ 4.1 ± 3.1	14 ± 1.8/ 11 ± 1.9	2.4 ± 2.1/ 2.4 ± 0.11	1.7 ± 1.93/ 1.4 ± 1.81	4.1 ± 0.58/ 3.6 ± 3.9	2.4 ± 3.3/ 2.3 ± 2.8	2.6 ± 3.4/ 2.4 ± 3.1	2.4 ± 1.06/ 7.5 ± 4.8
PSNR	40 ± 2.1/ 42 ± 1.6	15 ± 4.1/ 16 ± 3.1	19 ± 2.1/ 17 ± 3.3	27.7 ± 1.1/ 30 ± 1.2	14 ± 0.9/ 9 ± 1.3	16 ± 1.4/ 17 ± 2.1	38 ± 9/ 41 ± 4.5	11 ± 1.1/ 10 ± 1.5	16 ± 2.3/ 17 ± 2.6	44 ± 4.3/ 34 ± 6.7
ERR3	5.7 ± 2.2/ 3.4 ± 0.7	4.5 ± 4.4/ 5.3 ± 2.6	4.9 ± 4.7/ 4.4 ± 5.3	6.6 ± 2.8/ 15 ± 2.8	8.9 ± 2.1/ 19 ± 3.7	11.7 ± 1.63/ 12 ± 2.7	10.8 ± 1.1/ 5.6 ± 4.9	6.4 ± 4.3/ 9 ± 3	8.6 ± 3.4/ 8 ± 3.1	3.1 ± 1.3/ 9.2 ± 5.9
ERR4	8.9 ± 4.8/ 4.6 ± 1.1	6.5 ± 2.4/ 6.5 ± 2.2	49.4 ± 3.7/ 5 ± 4.1	41 ± 1.9/ 19 ± 3.7	11.2 ± 3.2/ 10.5 ± 3.1	9.7 ± 2.2/ 9 ± 5.1	20.7 ± 2.1/ 8 ± 6.4	7.4 ± 6.1/ 9 ± 7	9.5 ± 4.4/ 9.1 ± 4.2	3.5 ± 1.5/ 10 ± 6.3
Q	0.95 ± 0.01/ 0.95 ± 0.08	0.6 ± 0.4/ 0.5 ± 0.03	0.4 ± 0.7/ 0.5 ± 0.6	0.7 ± 0.33/ 0.65 ± 0.38	0.2 ± 0.3/ 0.4 ± 0.4	0.67 ± 0.5/ 0.7 ± 0.6	0.93 ± 0.02/ 0.9 ± 0.08	0.6 ± 0.46/ 0.7 ± 0.5	0.5 ± 0.4/ 0.5 ± 0.3	0.8 ± 0.05/ 0.88 ± 0.09
SSI	0.97 ± 0.01/ 0.98 ± 0.06	0.56 ± 0.6/ 0.6 ± 0.05	0.5 ± 0.5/ 0.6 ± 0.4	0.79 ± 0.03/ 0.84 ± 0.04	0.29 ± 0.23/ 0.35 ± 0.33	0.7 ± 0.4/ 0.72 ± 0.5	0.97 ± 0.002/ 0.96 ± 0.06	0.5 ± 0.6/ 0.56 ± 0.7	0.6 ± 0.5/ 0.67 ± 0.7	0.95 ± 0.03/ 0.88 ± 0.08
AD	0.16 ± 0.01/ 0.09 ± 0.03	0.11 ± 0.06/ 0.10 ± 0.04	0.5 ± 0.05/ 0.6 ± 0.04	0.23 ± 0.22/ 0.99 ± 0.01	0.22 ± 0.02/ 0.35 ± 0.03	0.37 ± 0.03/ 0.33 ± 0.02	0.05 ± 0.01/ 0.99 ± 0.05	0.45 ± 0.07/ 0.55 ± 0.06	0.36 ± 0.25/ 0.47 ± 0.04	0.8 ± 0.05/ 0.9 ± 0.01
SC	1 ± 0.06/ 1 ± 0.03	1.1 ± 0.06/ 0.9 ± 0.04	0.6 ± 0.05/ 0.5 ± 0.04	0.98 ± 0.007/ 0.99 ± 0.01	0.31 ± 0.03/ 0.35 ± 0.02	0.45 ± 0.04/ 0.54 ± 0.03	1 ± 0.004/ 1 ± 0.005	0.54 ± 0.05/ 0.55 ± 0.04	0.63 ± 0.45/ 0.67 ± 0.47	1 ± 0.002/ 0.87 ± 0.1
NCC	0.99 ± 0.03/ 0.99 ± 0.02	0.87 ± 0.06/ 0.79 ± 0.03	0.05 ± 0.04/ 0.04 ± 0.03	0.99 ± 0.005/ 0.99 ± 0.005	0.62 ± 0.02/ 0.67 ± 0.04	0.44 ± 0.04/ 0.51 ± 0.05	0.99 ± 0.012/ 0.99 ± 0.001	0.31 ± 0.03/ 0.49 ± 0.03	0.53 ± 0.07/ 0.61 ± 0.08	0.99 ± 0.01/ 1 ± 0.06
MD	82 ± 62/ 30 ± 12	36 ± 17/ 35 ± 15	42 ± 23/ 39 ± 22	119 ± 17/ 94 ± 18	25 ± 28/ 20 ± 22	33 ± 2.2/ 37 ± 20	35 ± 17/ 43 ± 27	29 ± 19/ 31 ± 12	34 ± 16/ 27 ± 11	13 ± 5/ 38 ± 15

GAE: geometric average error, MSE: mean square error, SNR: signal to noise ratio, RMSE: root mean square error, PSNR: peak signal to noise ratio, Err3, Err4: Minkowski metrics, Q: Universal quality index, SSI: structural similarity index, AD: average difference, SC: structural content, NCC: normalized cross correlation, MD: maximum difference.

Table 3, that compared with the rest of the filters investigated in this study, the despeckle filter DsFlsmv has the best performance in terms of Q ($0.95 \pm 0.01/0.95 \pm 0.08$) and SSI ($0.97 \pm 0.01/0.98 \pm 0.06$) applied to the whole or in an ROI (–/–) respectively. Moreover, by observing all the image quality evaluation metrics presented in Table 3 it can be concluded that the DsFlsmv leads in performance when applied in an ROI, followed by the despeckle filter DsFhmedian. Another conclusion is that that all the image quality evaluation metrics presented in Table 3 are equally important. It should also be stressed that a higher values for the SNR or PSNR (or equivalently, a lower MSE or RMSE) do not necessarily point to a higher subjective image quality, although they do provide some indication.

4.4. *Visual evaluation by the expert*

Table 4 presents the results of the visual evaluation for the 100 original and despeckled CCA ultrasound images, made by a neurovascular specialist. The evaluation was performed on both the entirely despeckled image as well as in an ROI, where both methods gave similar visual evaluation scorings. The Table presents the overall average percentage (%) score assigned by the expert for each filter as well as the filter ranking. It is observed that the DsFlsmv is marginally the best image despeckle filter, with a score of 91%, followed by the filter DsFhmedian and DsFkuwahara with scores of 90% and 83% respectively. The rest of the filters had a poorer performance.

Table 4 – Percentage scoring of visual evaluation of the original and despeckled images by the expert.

Expert	Original	DsFlsmv	DsFwiener	DsFlsmisc	DsFkuwahara	DsFgf	DsFmedian	DsFhmedian	DsFad	DsFnldif	DsFsrad
Neurovascular specialist	82	91	71	74	83	73	76	90	77	75	79
Ranking		1	10	8	3	9	6	2	5	7	4

5. Discussion

In this work we present an IDF software system for despeckling ultrasound images of the CCA, with the goal to reduce multiplicative noise in ultrasound images of the CCA in order to increase the visual perception by the expert/s, as well as to make the images suitable for further analysis tasks, such as image segmentation, texture analysis, image compression, and coding. The IDF software system was evaluated by a medical expert and it was also used in a number of other studies performed by our group described in [4,5,12] and also presented in Table 1, where despeckle filtering was applied to increasing the visual perception evaluation of the medical expert.

The proposed IDF system can also applied for normalization of ultrasound imaging, as it is described in this study and is also documented in other studies performed by our group [3–5], [12–19]. It was shown in [12], that ultrasound image normalization applied before despeckle filtering, improves the image quality to assist the visual evaluation by experts. In [13–15] image despeckle filtering was applied prior to the segmentation of the IMC in ultrasound images of the CCA, and the segmentation of the atherosclerotic carotid plaque. In [18], normalization was applied for the generation of the M-mode image from ultrasound videos of the CCA, whereas in [17], normalization was applied prior video despeckle filtering of the carotid and prior the segmentation of the IMC [39], and the atherosclerotic carotid plaque [19] from ultrasound videos of the CCA.

While there are a number of commercially available software packages for denoising and/or analyzing ultrasound

images [10,11,40,41], we found no other studies where an integrated software similar with the one presented in this study was proposed. The DsFlsmv filter, found to perform the best in this study, was also found to perform better than other despeckle filters in two different studies presented by our group [5,12]. It was also used to increase the accuracy of the segmentation of the atherosclerotic carotid plaque [15], the IMC [14], and the media and the intima layers [13] of the CCA. In [24], the Ultra3D® image processing and visualization software package incorporates additive median noise image filtering to increase the optical perception evaluation. The Usimagetool® [25] that is suitable for processing and visualization of 2D and 3D ultrasound images, incorporates speckle reducing anisotropic diffusion [33], as well as a number of other additive noise filters. Additionally, there are a number of other software systems available in the market for the segmentation of the IMC in ultrasound images of the CCA [20,21,23] (Segment™, Atheroedge™, Royal Perth IMT software and M'Ath®), where image despeckle filtering is not incorporated. Finally, in [22] a software system for the manual delineation, and automated image normalization and texture analysis of the atherosclerotic carotid plaque in ultrasound images of the CCA was presented.

Speckle is not truly a noise in the typical engineering sense because its texture often carries useful information about the image being viewed [26,42]. It is the primary factor that limits the contrast resolution in diagnostic ultrasound imaging, thereby limiting the detectability of small, low-contrast lesions, and making the ultrasound images generally difficult for the non-specialist to interpret [5,26,27,29]. Due to the speckle presence, ultrasound experts with insufficient experience may not often draw useful conclusions from the images [3,4]. Speckle noise also limits the effective application of image processing and analysis algorithms (i.e. edge detection, segmentation) and display in 2D and volume rendering in 3D. Therefore, speckle is most often considered as a dominant source of noise in ultrasound imaging and should be filtered out [26–28], without affecting important features of the image. In [43], where a review on ultrasound image segmentation methods is presented, it is discussed whether speckle should be treated as noise or a feature. It was concluded that from a segmentation perspective, you may choose to remove it or utilize it for the information it contains. Speckle reduction filtering of the CCA was also proposed by [3–5,12–19] where it was shown that this improves the image quality and the visual evaluation of the image. However, in other segmentation studies for extracting the carotid artery plaque borders in intra-vascular ultrasound (IVUS) imaging, speckle was used as useful information [42,44]. Table 2 showed that most of the features presented in this study are preserved after filtering, while at the same time the optical perception evaluation is improved. It should be also noted that due to specific character of some echo images, speckle directionality should also be considered by estimating appropriate texture features from the area of interest [45]. Such an approach will ensure that texture features carry information that it is not biased by speckle orientation.

It was also documented in other studies [1,4,11,21,30,33], that the MSE, RMSE, SNR and PSNR measures are not objective for image quality evaluation and that they do not correspond to all aspects of the visual perception nor they correctly reflect artifacts [1]. Recently, the Q and SSI [1] measures have also been proposed for objective image quality evaluation. It is also important to note that the proposed IDF toolbox consists of a combination of subjective and objective measures that should be used in combination for proper image quality evaluation results [5,12].

We have found in the technical literature numerous detailed examples of 2D algorithms for reducing speckle and improving image quality of ultrasound images but there is relatively little information available on the commercial image processing techniques employed in practice, such as Speckle Reduction Imaging (GE Healthcare, Milwaukee, WI), Xtreme Resolution (Philips Healthcare, Bothell, WA) and, indeed, the methods evaluated in this paper. The proposed IDF software tool may help toward this direction and could be utilized as a complementary tool in the clinical praxis.

Some other software packages proposed recently in the literature and freely made available as standalone packages have been developed for the automatic classification and segmentation of 2D/3D medical images [46], the segmentation of the IMC in ultrasound images [47], DICOM series of ultrasound images of the CCA [48], as well as for image texture analysis [49].

5.1. *Limitations of the image despeckling method*

There are some limitations in the proposed methodology which are summarized below. MATLAB® is not the most computationally efficient environment. However, most of the implemented algorithms, programmed in MATLAB® are sufficiently adequate, in particular in and manually defining and despeckling structures, as well as if the users can effectively define ROI and crop images to reduce the image dimensions using the available tools in the software. Therefore, computation speed is not a limiting factor for our software tool as the filtering can also be applied in an ROI.

Another issue is that some automatic algorithms use many user-configurable parameters, such as the size of the moving window, the number of iterations and the coefficient of variation and is left to the user to choose the best parameter values. In this application we have chosen default initial parameter values based on our experience. However, in many scenarios these parameters may still need to be changed by the user to achieve optimal results.

Validation of the final results is one of the most challenging tasks in medical image analysis applications. Results are usually compared with the optical perception evaluation by specialists, as it is also done in this study. It is true that such comparisons are often affected by other issues, such as, for example, inter- and intra-observer variability [3–12]. However, it is relatively safe to consider automated methods as second opinions intended to aid the user. This practice has been shown to be useful in many Computed Aided Design applications.

It should be noted that the processing time of the proposed method could be further reduced by applying despeckle filtering only on selected areas of the image. Furthermore, software optimization methods (i.e. the MATLAB® software optimization toolbox) could be investigated for increasing the

performance of the proposed IDF software system. Finally, it should be noted that the proposed methods could also be applied to other applications, such as echocardiography but a direct comparison of the results produces with this study will not be possible as different results will be produced with a different database.

6. Concluding remarks

In this paper, a freeware despeckle filtering toolbox for ultrasound images has been presented that can be downloaded from (http://www.cs.ucy.ac.cy/medinfo/). The software toolbox proposed in this study is based on the following 10 despeckle filters, DsFlsmv, DsFwiener, DsFlsminsc, DsFkuwahara, DsFgf, DsFmedian, DsFhmedian, DsFad, DsFnldif and DsFsrad. The toolbox also supports image normalization, manual delineation of structures, extraction of textures and quantitative evaluation metrics between the original and the despeckled images, as well as qualitative evaluation by experts, where all computed results are saved in a file for further use. The system was evaluated on atherosclerotic carotid plaque ultrasound images, where it was shown that the filters DsFlsmv, and DsFhmedian improved image quality perception (based on the expert's assessment and the quantitative image quality metrics). It is anticipated that the system could help the physician in the assessment of cardiovascular image analysis. However, exhaustive evaluation of the despeckle filtering toolbox has to be carried out by more experts on more image samples.

REFERENCES

[1] Z. Wang, A. Bovik, H. Sheikh, E. Simoncelli, Image quality assessment: from error measurement to structural similarity, IEEE Trans. Image Process. 13 (4) (2004) 600–612.

[2] T. Elatrozy, A. Nicolaides, T. Tegos, A. Zarka, M. Griffin, M. Sabetai, The effect of B-mode ultrasonic image standardization of the echodensity of symptomatic and asymptomatic carotid bifurcation plaque, Int. Angiol. 17 (3) (1998) 179–186.

[3] C.P. Loizou, Ultrasound Image Analysis of the Carotid Artery, Applications in Ultrasound Filtering, Segmentation and Texture Analysis, Lambert Academic Publishing GmbH & Co. KG, Saarbruecken, Germany, 2012.

[4] C.P. Loizou, C.S. Pattichis, Despeckle Filtering Algorithms and Software for Ultrasound Imaging. Synthesis Lectures on Algorithms and Software for Engineering, Morgan & Claypool Publishers, San Rafael, CA, USA, 2008.

[5] C.P. Loizou, C.S. Pattichis, C.I. Christodoulou, R.S.H. Istepanian, M. Pantziaris, A.N. Nicoliades, Comparative evaluation of despeckle filtering in ultrasound imaging of the carotid artery, IEEE Trans. Ultrason. Feroelctr. Freq. Control 52 (2) (2005) 1653–1669.

[6] C.M. Wu, Y.C. Chen, K.-S. Hsieh, Texture features for classification of ultrasonic images, IEEE Trans. Med. Imaging 11 (1992) 141–152.

[7] C.I. Christodoulou, C.S. Pattichis, M. Pantziaris, A.N. Nicolaides, Texture-based classification of atherosclerotic carotid plaques, IEEE Trans. Med. Imaging 22 (7) (2003) 902–912.

[8] R.M. Haralick, K. Shanmugam, I. Dinstein, Texture features for image classification, IEEE Trans. Syst. Man Cybernet. 3 (1973) 610–621.

[9] E. Kyriakou, M.S. Pattichis, C. Christodoulou, C.S. Pattichis, S. Kakkos, M. Griffin, A.N. Nicolaides, Ultrasound imaging in the analysis of carotid plaque morphology for the assessment of stroke, in: J.S. Suri, C. Yuan, D.L. Wilson, S. Laxminarayan (Eds.), Plaque Imaging: Pixel to Molecular Level, IOS Press, Amsterdam, Netherlands, 2005, pp. 241–275.

[10] J. Grosby, B.H. Amundsen, T. Hergum, E.W. Remme, S. Langland, H. Trop, 3D speckle tracking for assessment of regional left ventricular function, Ultrasound Med. Biol. 35 (2009) 458–471.

[11] J.A. Noble, N. Navab, H. Becher, Ultrasonic image analysis and image quided interventions, Interface Focus 1 (2011) 673–685.

[12] C.P. Loizou, C.S. Pattichis, M. Pantziaris, T. Tyllis, A.N. Nicolaides, Quality evaluation of ultrasound imaging in the carotid artery based on normalization and speckle reduction filtering, Med. Biol. Eng. Comput. 44 (5) (2006) 414–426.

[13] C.P. Loizou, C.S. Pattichis, A.N. Nicolaides, M. Pantziaris, Manual and automated media and intima thickness measurements of the common carotid artery, IEEE Trans. Ultrasound Ferroelectr. Freq. Control 56 (5) (2009) 983–994.

[14] C.P. Loizou, C.S. Pattichis, M. Pantziaris, T. Tyllis, A.N. Nicolaides, Snakes based segmentation of the common carotid artery intima media, Med. Biol. Eng. Comput. 45 (1) (2007) 35–49.

[15] C.P. Loizou, C.S. Pattichis, M. Pantziaris, A.N. Nicolaides, An integrated system for the segmentation of atherosclerotic carotid plaque, IEEE Trans. Inform. Technol. Biomed. 11 (6) (2007) 661–667.

[16] C.P. Loizou, C. Theofanous, M. Pantziaris, T. Kasparis, P. Christodoulides, A.N. Nicolaides, C.S. Pattichis, Despeckle filtering toolbox for medical ultrasound video, Int. J. Monitor. Surveillance Technol. Res. (IJMSTR) 4 (1) (2014) 61–79, Oct.-Dec. 2013 (Special issue on Biomedical Monitoring Technologies).

[17] C.P. Loizou, T. Kasparis, P. Christodoulides, C. Theofanous, M. Pantziaris, E. Kyriakou, C.S. Pattichis, Despeckle filtering in ultrasound video of the common carotid artery, in: 12th International Conference on Bioinformatics & Bioengineering Processing (BIBE), Larnaca, Cyprus, November 11–13, 2012, p. 4.

[18] C.P. Loizou, M. Pantziaris, C.S. Pattichis, E. Kyriakou, M-mode state-based identification in ultrasound videos of the common carotid artery, in: Proceedings of 4th International Symposium on Communication Control & Signal Processing, ISCCSP, Limassol, Cyprus, March 3–5, 2010, p. 6.

[19] C.P. Loizou, C.S. Pattichis, S. Petroudi, M. Pantziaris, T. Kasparis, A.N. Nicolaides, Segmentation of atherosclerotic carotid plaque in ultrasound video, in: 34th Annual International Conference on IEEE Engineering Medicine and Biology, EMBC, San Diego, USA, August 28–September 1, 2012, p. 4.

[20] P.H. Davis, J.D. Dawson, M.B. Biecha, R.K. Mastbergen, M. Sonka, Measurement of aortic intimal-media thickness in adolescents and young adults, Ultrasound Med. Biol. 36 (4) (2010) 560–565.

[21] E. Heiberg, J. Sjogren, M. Ugander, M. Carlsson, H. Engblom, K. Arheden, Design and validation of a segment-freely available software for cardiovascular image analysis, BMC Med. Imaging 10 (1) (2010) 1–13.

[22] E.C. Kyriakou, C.S. Pattichis, M.A. Karaolis, C.P. Loizou, M.S. Pattichis, S. Kakkos, A.N. Nicolaides, An integrated system for assessing stroke risk, IEEE Eng. Med. Biol. Mag. 26 (5) (2007) 43–50.

[23] F. Molinari, K.M. Meiburger, J. Suri, Automated high-performance cIMT measurement techniques using patented AtheroEdge™: a screening and home monitoring system, in: 33rd Annual International Conference on IEEE EMBS, Boston, USA, 2011, pp. 6651–6654.
[24] X.G. Xu, Y.H. Na, T. Zhang, Design and test of a PC-based 3D ultrasound software system Ultra3D, Comp. Biol. Med. 38 (2) (2008) 244–251.
[25] R. Cardenes-Almeida, A. Tristan-Vega, G.V.-S. Ferrero, S.A. Fernandez, et al., Usimagtool: an open source freeware software for ultrasound imaging and elastography, in: International Work on Multimodal Interfaces, eNTERFACE, Istambul, Turkey, 2007, pp. 117–127.
[26] J.S. Lee, Digital image enhancement and noise filtering by using local statistics, IEEE Trans. Pattern Anal. Mach. Intell. PAMI-2 2 (1980) 165–168.
[27] V.S. Frost, J.A. Stiles, K.S. Shanmungan, J.C. Holtzman, A model for radar images and its application for adaptive digital filtering of multiplicative noise, IEEE Trans. Pattern Anal. Mach. Intell. 4 (2) (1982) 157–165.
[28] M. Kuwahara, K. Hachimura, S. Eiho, M. Kinoshita, in: K. Preston, M. Onoe (Eds.), Digital Processing of Biomedical Images, Plenum Publishing Corporation, New York, 1976, pp. 187–203.
[29] L.J. Busse, T.R. Crimmins, J.R. Fienup, A model based approach to improve the performance of the geometric filtering speckle reduction algorithm, in: IEEE Ultrasonic Symposium, 1995, pp. 1353–1356.
[30] A. Nieminen, P. Heinonen, Y. Neuvo, A new class of detail-preserving filters for image processing, IEEE Trans. Pattern Anal. Mach. Intell. 9 (1987) 74–90.
[31] P. Perona, J. Malik, Scale-space and edge detection using anisotropic diffusion, IEEE Trans. Pattern Anal. Mach. Intell. 12 (7) (1990) 629–639.
[32] A. Panayides, M.S. Pattichis, C.S. Pattichis, C.P. Loizou, M. Pantziaris, A. Pitsillides, Atherosclerotic plaque ultrasound video encoding, wireless transmission, and quality assessment using H.264, IEEE Trans. Inform. Technol. Biomed. 15 (3) (2001) 387–397.
[33] Y. Yongjian, S.T. Acton, Speckle reducing anisotropic diffusion, IEEE Trans. Image Process. 11 (11) (2002) 1260–1270.
[34] A Philips medical system company, Comparison of image clarity, SonoCT Real-time Compound Imaging Versus Conventional 2D Ultrasound Imaging, ATL Ultrasound Report, 2001.
[35] A.N. Nicolaides, M. Sabetai, S.K. Kakkos, S. Dhanjil, T. Tegos, J.M. Stevens, The asymptomatic carotid stenosis and risk of stroke study, Int. Angiol. 22 (3) (2003) 263–272.
[36] J.S. Weszka, C.R. Dyer, A. Rosenfield, A comparative study of texture measures for terrain classification, IEEE Trans. Syst. Man Cybernet. 6 (1976) 269–285.
[37] M. Amadasun, R. King, Textural features corresponding to textural properties, IEEE Trans. Syst. Man Cybernet. 19 (5) (1989) 1264–1274.
[38] D.G. Altman (Ed.), Practical Statistics for Medical Research, Chapman & Hall, London, 1991.
[39] C.P. Loizou, T. Kasparis, P. Papakyriakou, L. Christodoulou, M. Pantziaris, C.S. Pattichis, Video segmentation of the common carotid artery intima-media complex, in: 12th International Conference on Bioinformation & Bioengineering Process (BIBE), Larnaca, Cyprus, November 11–13, 2012, p. 4.
[40] V. Zlokolica, W. Philips, van de Ville, Robust non-linear filtering for video processing, IEEE Proc. Vision Imag. Signal. Process. 2 (2) (2002) 571–574.
[41] V. Zlokolica, A. Pizurica, W. Philips, Recursive temporal denoising and motion estimation of video, Int. Conf. Image Process. 3 (3) (2008) 1465–1468.
[42] E. Brusseau, C.L. De Korte, F. Mastick, J. Schaar, A.F.W. van der Steen, Fully automatic luminal contour segmentation in intracoronary ultrasound imaging – a statistical approach, IEEE Trans. Med. Imaging 23 (5) (2004) 554–566.
[43] J.A. Noble, A. Boukerroui, Ultrasound image segmentation: a survey, IEEE Trans. Med. Imaging 25 (8) (2006) 987–1010.
[44] A. Fenster, A. Zahalka, An automated segmentation method for three-dimensional carotid ultrasound images, Phys. Med. Biol. 46 (2001) 321–1342.
[45] L. Chrzanowski, J. Drozdz, M. Strzelecki, M. Krzeminska-Pakula, K.S. Jedrzejewski, J.D. Kasprzak, Application of neural networks for the analysis of intravascular ultrasound and histological aortic wall appearance – an in vitro tissue characterisation study, Ultrasound Med. Biol. 34 (1) (2008) 103–113.
[46] M. Strzelecki, P. Szczypinski, A. Materka, A. Klepaczko, A software tool for automatic classification and segmentation of 2D/3D medical images, Nucl. Instrum. Method Phys. Res. 702 (2013) 137–140.
[47] A.M.F. Santos, R.M. Dos Santos, P.M.A. Castro, E. Azevedo, et al., A novel algorithm for the segmentation of the lumen of the carotid artery in ultrasound B-mode images, Expert Syst. Appl. 40 (2013) 6570–6579.
[48] K. Potter, D.J. Green, C.J. Reed, R.J. Woodman, et al., Carotid intima-media thickness measured on multiple ultrasound frames; evaluation of a DICOM-based software system, Cardiovasc. Ultrasound 5 (29) (2007) 1–10.
[49] P.M. Szczypiński, M. Strzelecki, A. Materka, A. Klepaczko, MaZda – a software package for image texture analysis, Comp. Methods Prog. Biomed. 94 (1) (2008) 66–76.